Analysis of Fe XXI Spectral Lines Measured in LHD Plasma

Izumi MURAKAMI, Hiroyuki A. SAKAUE, Norimasa YAMAMOTO[1], Daiji KATO,
Shigeru MORITA and Tetsuya WATANABE[2]

National Institute for Fusion Science, 322-6 Oroshi-cho, Toki, 509-5292, Japan
[1]*Institute of Laser Engineering, Osaka University, Suita, Oasaka 565-0871, Japan*
[2]*National Astronomical Observatory, Mitaka, Tokyo 181-8588, Japan*

We measured extreme ultraviolet spectra of plasmas in the Large Helical Device after an Fe pellet was injected and analyzed the Fe XXI spectral lines λ 12.12 nm ($2s^22p^2$ $^3P_2$-$2s2p^3$ $^3P_2$) and λ 12.875 nm ($2s^22p^2$ $^3P_0$-$2s2p^3$ $^3D_1$). By constructing a collisional-radiative model for Fe XXI, we obtained the electron density dependence of the line intensity ratio, which is the result of the excitation process among the fine-structure levels of the ground state, $2s^22p^2$ ^3P_J by electron and proton impact. Using the obtained electron density dependence, we estimated the electron density from the measured intensity ratio. By comparing the estimated density with the electron density distribution measured by a far infrared interferometer, we could estimate the location of the Fe XXI emitting region. We found that Fe XXI appeared first around the density peak formed by the pellet and later expanded toward a low-density region. The corresponding electron temperature of the location is lower than that for ionization equilibrium, and the Fe XXI ions are expected to be in a non-equilibrium ionization state.

1. Introduction

Iron is one of the major impurities in various plasmas, since iron ions are provided by stainless-steel vessel walls in laboratory plasmas or produced as a product of nucleosynthesis in the core of a star or during supernova explosion in astrophysical plasmas. In astrophysical plasmas, in particular, iron is abundant and is an important index for heavy element abundance. It is important to measure the intensity of iron ion spectral lines and determine the physical condition of plasmas precisely by spectroscopic methods.

Many studies have been conducted for modeling the spectral line intensity ratios of Fe ions for plasma diagnostics. Doschek *et al.* (1973) first revealed the possibility of using Fe XXII lines as a density diagnostic for solar flares [1], and Mason and Storey (1980) calculated the electron density dependences of some Fe XXII line intensity ratios with improved atomic data [2]. Mason *et al.* (1979) first calculated the Fe XXI line ratio [3] for electron density diagnostics; updated calculations with improved atomic data were later reported [4, 5].

To analyze Fe ion spectral lines measured in solar plasmas by the Extreme-ultraviolet Imaging Spectrometer (EIS) mounted on the HINODE solar satellite [6], we have developed a set of collisional-radiative (CR) models for Fe ions from H-like to Ca-like ions for plasma diagnostics. A CR model provides the population densities of excited levels and spectral line intensities. To verify the validity of the

model, we measured Fe spectral lines in laboratory plasmas and applied the model for analysis. We examined Fe XIII lines measured for plasmas in the Large Helical Device (LHD) and in an electron beam ion trap (EBIT) and compared with the CR model for Fe XIII to verify it [7]. Using the verified CR model, the electron density distribution was estimated using the Fe XIII line intensity ratios for a solar active region [8]. Fe XXII lines were also measured in LHD and EBIT plasmas and used to check the CR model for Fe XXII [9].

In this paper we focus on Fe XXI spectral lines of C-like Fe ions (Fe^{20+}). These ions are produced in plasma with electron temperature $T_e \sim 1$ keV and have been observed in solar flares [10]. We measured extreme ultraviolet (EUV) spectra of LHD plasmas and found Fe XXI lines and other L-shell Fe ion lines. Here we focus on two lines, λ 12.12 nm ($2s^22p^2$ $^3P_2$-$2s2p^3$ $^3P_2$) and λ 12.875 nm ($2s^22p^2$ $^3P_0$-$2s2p^3$ $^3D_1$). The intensity ratio of these lines shows the electron density dependence and can be used for density diagnostics [3–5]. We calculate the electron density dependence of the intensity ratio (Section 3) and compare it with the measured EUV spectra of the LHD plasma (Section 4). We then discuss the emission region of Fe XXI ions estimated using the result (Section 5). Section 6 concludes the paper.

2. EUV Spectra Measurement

EUV spectra in the 8-26 nm wavelength range were measured for plasmas in the LHD using the flat-field EUV
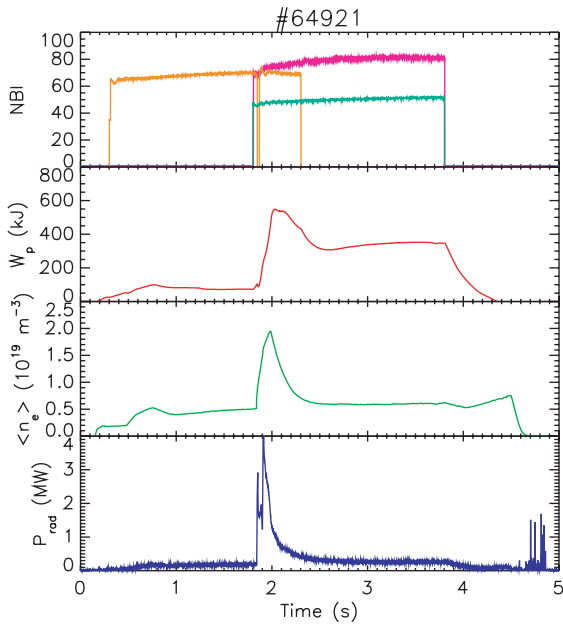
author's e-mail: murakami.izumi@nifs.ac.jp

Fig. 1 Temporal evolution of the discharge of shot 64921 for NBI power, stored energy W_{p}, line-averaged electron density $\langle n_{\mathrm{e}} \rangle$, and total radiated power P_{rad}.
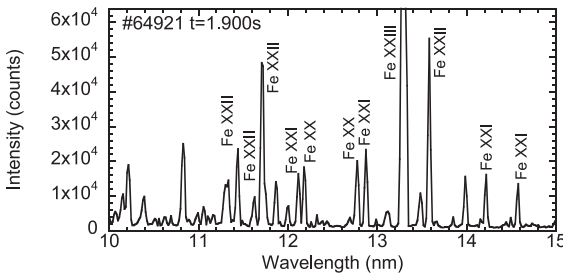

Fig. 2 EUV spectrum of shot 64921 at $t = 1.9$ s.

spectrometer [11]. The exposure time of one frame was 5 ms. We analyzed the spectra measured for the plasma of shot number 64921, in which an iron pellet was injected at $t = 1.8$ s. Plasma was heated by neutral beam injection (NBI). Figure 1 shows the temporal evolution of the discharge.

After Fe pellet injection, M-shell Fe ions appeared first; L-shell Fe ions then appeared at $t = 1.875$ s and lasted until $t \sim 2$ s when line intensities weakened to an intensity similar to that of background Fe ion lines originating from the vacuum vessel. Figure 2 shows the EUV spectrum at $t = 1.9$ s. The line intensities of λ 12.12 nm and λ 12.875 nm lines were obtained by fitting with a Gaussian profile. Figure 3 shows the obtained temporal distribution of the line intensities and the intensity ratio. The intensity reached maximum at $t \sim 1.89$ s and then decreased. However, the intensity ratio was nearly constant until $t \sim 1.95$ s and then decreased.
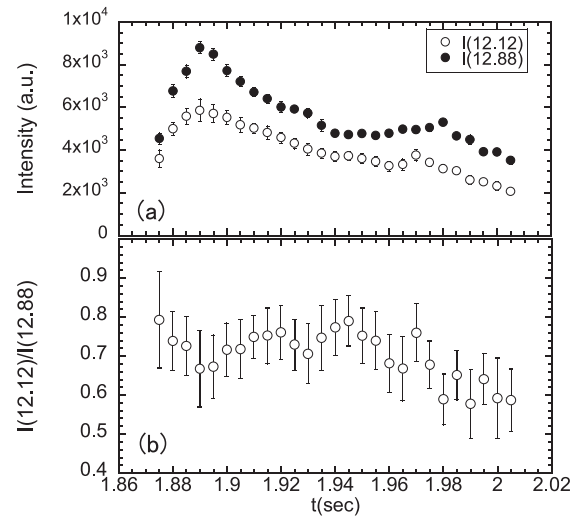

Fig. 3 Temporal distribution of (a) the line intensities of $I(\lambda\, 12.12\ \mathrm{nm})$ and $I(\lambda\, 12.88\ \mathrm{nm})$ and (b) the line intensity ratio.

3. CR Model

The CR model for Fe XXI was constructed including excited fine-structure levels with the principal quantum number n up to 5. The rate equations for all excited levels are solved assuming a quasi-steady state. The rate equation for the population density of level p, $n(p)$, is described as

$$\frac{\mathrm{d}n(p)}{\mathrm{d}t} = \sum_q W(q, p)n(q) - \sum_q W(p, q)n(p) = 0, \qquad (1)$$

where $W(p, q)$ is the rate coefficient of atomic processes for the transition from level p to level q. All relevant atomic processes were considered in the rate equations: radiative decay, electron-impact excitation and de-excitation, electron-impact ionization, radiative recombination, dielectronic recombination, three-body recombination, and proton-impact excitation and de-excitation. Most of the atomic data were calculated using the HULLAC atomic code [12]. The wavelengths of spectral lines for some important dipole transitions were obtained from the NIST database [13]. Proton-impact excitation rate coefficients were obtained from the evaluated data [14]. For electron-impact excitation rate coefficients, we examined two models. In one, the rate coefficients calculated by the HULLAC code were used for all transitions (the Hullac model). In the other, the rate coefficients for transitions between $n = 2$-2 and 2-3 levels were replaced with data obtained in Ref. [15], in which the R-matrix method was used for the calculation (the RMaX model). The R-matrix method can include the effect of resonance and provide better rate coefficients for low temperature regions than the distorted wave method used in the HULLAC code. Proton-impact excitation is important for transitions among fine-structure levels of the ground state, $2s^2 2p^2\ {}^3P_J$, where $J = 0$, 1, and 2. The proton temperature (T_{p}) is assumed to be the same as the electron temperature (T_{e}) and for the proton den-
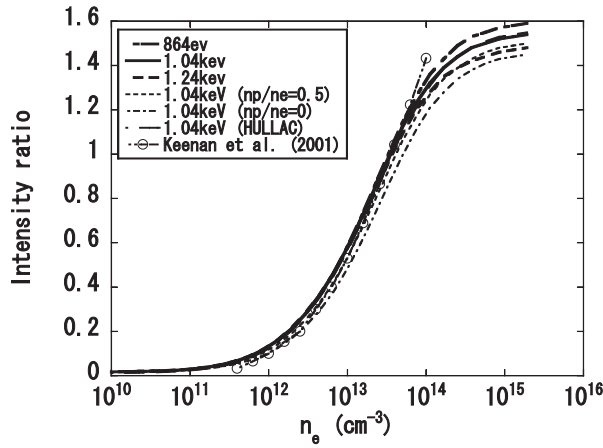
Fig. 4 Calculated intensity ratio as a function of electron density for the RMaX model with $n_p/n_e = 1$ and $T_e = 864$ eV (thick long-dashed line), 1.04 keV (thick solid line), and 1.24 keV (thick dashed line); the RMaX model with $n_p/n_e = 0.5$ and $T_e = 1.04$ keV (think dashed line); the RMaX model with $n_p/n_e = 0$ and $T_e = 1.04$ keV (thin dot-dashed line); the Hullac model with $n_p/n_e = 1$ and $T_e = 1.04$ keV (think long-rdashed line); and $T_e = 10^7$ K model of Ref. [5] (solid circles).

Fig. 5 Temporal distribution of (a) electron density estimated from the measured intensity ratio and CR model, and (b) normalized radius ρ of the location of the emitting region for different models: the RMaX model with $T_e = 1.04$ keV and $n_p/n_e = 0$ (solid triangles), 0.5 (solid squares), and 1 (solid circles), and the HULLAC model with $T_e = 1.04$ keV and $n_p/n_e = 1$ (open circles). Errors are shown only for the RMaX model with $n_p/n_e = 1$.

sity (n_p), we consider three cases: $n_p/n_e = 0$, 0.5, and 1, where n_e is the electron density. Regarding the effective collision strengths of the dominant processes for the two lines, for the population density of the upper level of the line $\lambda\,12.12$ nm, direct excitation from the $2s^2 2p^2\,^3P_0$ level is weak and excitation via the $2s^2 2p^2\,^3P_2$ level is strong. Thus, excitation from the $2s^2 2p^2\,^3P_0$ level to the $2s^2 2p^2\,^3P_2$ level by electron and proton impact is important, and this causes the electron density dependence of the intensity ratio.

The population density of excited level p is obtained as a combination of ionizing plasma component $n_1(p)$ and recombining plasma component $n_0(p)$:

$$n(p) = n_1(p) + n_0(p). \qquad (2)$$

The plasma considered here was heated by NBI and the population densities are dominated by the ionizing plasma component. The specific line intensity is obtained as $n(p)A_r(p,q)$, where $A_r(p,q)$ is the transition probability of the transition from level p to q.

By solving the rate equations, we obtained the electron density dependence of the line ratio, $I(\lambda\,12.12\,\text{nm})/I(\lambda\,12.88\,\text{nm})$ for a given electron temperature and proton density as shown in Fig. 4. The ratio has a quite weak electron temperature dependence for n_e less than 10^{14} cm^{-3}, less than 5% for $T_e \sim 0.6$-1.5 keV. Thus, this line intensity ratio can be used for density diagnostics for $n_e = 10^{12} \sim 10^{14}$ cm^{-3}. The difference between the different atomic data for the Hullac and RmaX models is also small within 10% for the above density region. The difference caused by the proton density is about 25% ($n_p/n_e = 0$) and 10% ($n_p/n_e = 0.5$). The ratio of Keenan
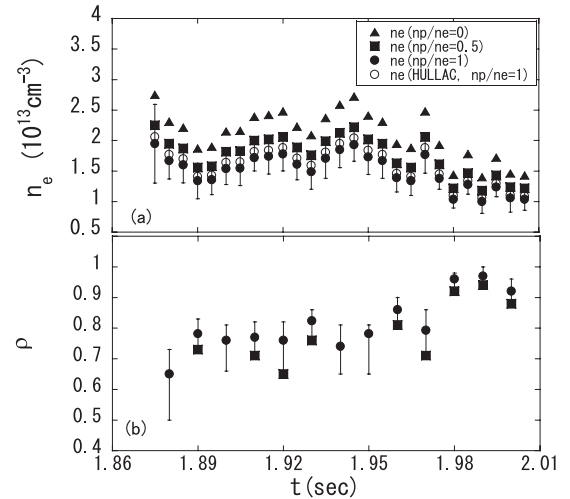
et al. [5] is larger than that of our model at 10^{14} cm^{-3} and smaller at $n_e < 10^{13}$ cm^{-3}. They did not mention about the proton temperature and density. The differences would be due to the different excitation rates and different number of levels considered in the model. The RMaX data used here are much improved over their data.

4. Analysis

By comparing the measured intensity ratios with the calculated relationship between the intensity ratio and the electron density, we can estimate the electron density.

Figure 5 (a) shows the temporal distribution of the estimated electron density of the Fe XXI emitting region. The estimated electron density is almost constant until $t \sim 1.95$ s and then decreases. As the figure shows, different electron densities are derived with different models. The differences are about 40% for the $n_p/n_e = 0$ and 1 and 17% for the $n_p/n_e = 0.5$ and 1 with the RMaX model. The difference between the RMaX and Hullac models is about 6% for $n_p/n_e = 1$. Hereafter, we use the RMaX model with $n_p/n_e = 1$.

By comparison with the electron density distribution measured by a far infrared (FIR) interferometer, we can estimate the location of the Fe XXI emitting region. Figure 6 shows the electron density distribution as a function of normalized minor radius ρ. The locations of the Fe XXI emitting region is also plotted every 0.01 s. At $t = 1.88$ s the location is estimated at around the local density peak $\rho \sim 0.65$. It remained at around $\rho \sim 0.75$ until $t \sim 1.97$ s and then moved towards $\rho \sim 1$. Figure 5 (b) shows the temporal distribution of the location and its motion. As
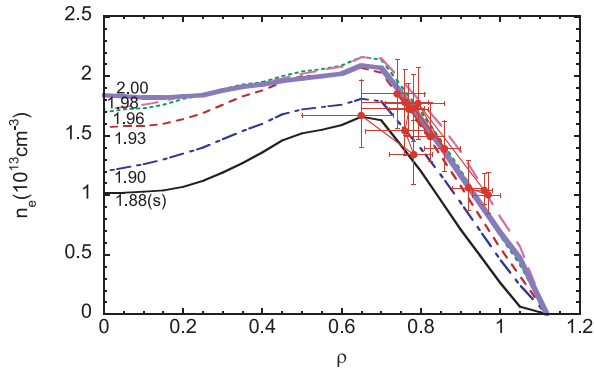
Fig. 6 Electron density distribution as a function of normal-ized radius, ρ, measured by the FIR interferometer at $t = 1.88$ s (thin solid line), 1.90 s (thin long dot-dashed line), 1.93 s (thin dashed line), 1.96 s (thin short dashed line), 1.98 s (long dashed line), and 2.00 s (thick solid line), with estimated location of Fe XXI emitting region (solid circles).

the location estimated using the RMaX model with $n_p/n_e = 0.5$ is shifted inward with a smaller ρ than in case of $n_p/n_e = 1$, as indicated by solid squares in Fig. 5 (b), the Fe XXI emitting region could be shifted inward if the local relative proton density n_p/n_e is smaller than 1.

5. Discussion

Using the estimated location of the Fe XXI emitting region, we can examine the electron temperature by comparing with the electron temperature distribution measured by Thomson scattering. This measured temperature distribution is asymmetric with respect to ρ, so it yields only approximate estimates. The Fe XXI emitting region first appeared at $T_e \sim 1.1$ keV and then shifted to $T_e \sim 0.7$ keV where it remained until $t \sim 1.97$ s; later it shifted to an even lower temperature region, $T_e \sim 0.5$ keV. The temperature here is lower than the abundance peak temperature of ionization equilibrium (low-density limit case) [16]. The ionization equilibrium distribution for the electron density around 10^{13}-10^{14} cm^{-3} could possibly be different from that in the low-density limit case. To check this assumption, we need to calculate the ion abundance of all Fe ions for the electron density region as future work. The other possibility is that the Fe XXI ions are not in ionization equilibrium due to expansion and diffusion caused by the bulk plasma after Fe pellet ablation. In future work, we need to calculate the time-dependent ion densities from the Fe pellet injection at $t = 1.8$ s until $t \sim 2$ s to check this possibility.

Two-dimensional measurements of EUV spectra in

the LHD plasma are planned for the near future. This will be a good tool to compare the Fe XXI emitting region directly with the estimated location using the method described in this paper. Such a comparison will prove the validity of the CR model and atomic data used in the model.

6. Conclusion

We measured EUV spectra in the LHD plasma and analyzed the Fe XXI spectral lines λ 12.12 nm and λ 12.88 nm. We constructed a CR model for Fe XXI and calculated the electron density dependence of the line intensity ratio. By comparing the calculated and measured intensity ratios, we estimated the electron density of the Fe XXI emitting region. Then, by comparison with the measured electron density distribution, we estimated the location of the emitting region, which appeared first at around the local density peak $\rho \sim 0.65$; it moved to $\rho \sim 0.75$, stayed there for a while, and moved again towards $\rho \sim 1$. The electron temperature of the emitting region was low, and we could expect that the ionization equilibrium temperature was lower than that expected for the low-density limit case, or the ions were not in ionization equilibrium. We will test these possibilities in future work.

[1] G. A. Doscheck et al., Solar Phys. **29**, 125 (1973).
[2] H. E. Mason and P. J. Storey, Mon. Not. R. Astron. Soc. **191**, 631 (1980).
[3] H. E. Mason et al., Astron. Astrophys. **73**, 74 (1979).
[4] F. P. Keenan et al., Solar Phys. **149**, 129 (1994).
[5] F. P. Keenan et al., Mon. Not. R. Astron. Soc. **326**, 1387 (2001)
[6] J. L. Culhane et al., Sol. Phys. **243**, 19 (2007).
[7] N. Yamamoto et al., Astrophys. J. **689**, 646 (2008).
[8] T. Watanabe et al., Astrophys. J. **692**, 1294 (2009).
[9] H. A. Sakaue et al., submitted to J. Appl. Phys. (2010).
[10] S. O. Kastner et al., Astrophys. J. **191**, 261 (1974).
[11] M. B. Chowduri et al., Rev. Sci. Instruments **78**, 023501 (2007).
[12] A. Bar-Shalon et al., J. Quant. Spect. Rad. Transf. **71**, 179 (2001).
[13] Yu. Ralchenko et al., http://physics.nist.gov/asd3 (2008).
[14] I. Skobelev et al., NIFS-DATA-99 (2007).
[15] N. Badnell et al., J. Phys. B **34**, 5071 (2001).
[16] P. Bryans et al., Astrophys. J. Suppl. **167**, 343 (2006).